PHYSICAL REVIEW A **93**, 012506 (2016)

Positronium decay from $n = 2$ states in electric and magnetic fields

A. M. Alonso, B. S. Cooper, A. Deller, S. D. Hogan, and D. B. Cassidy
Department of Physics and Astronomy, University College London, Gower Street, London WC1E 6BT, United Kingdom
(Received 26 November 2015; published 13 January 2016)

We report measurements and the results of calculations demonstrating that the annihilation dynamics of positronium (Ps) atoms can be controlled by Stark and Zeeman mixing of optically excited states. In the experiments a trap-based pulsed positron beam was employed to generate a dilute Ps gas with a density of $\sim 10^7$ cm^{-3} using a porous silica target. These atoms were excited via $1\,^3S_1 \rightarrow 2\,^3P_J$ transitions in parallel electric and magnetic fields using a nanosecond pulsed dye laser, and Ps annihilation was measured using single-shot lifetime spectroscopy. The composition of the excited $n = 2$ sublevels was controlled by varying the polarization of the excitation laser radiation and the strength of the electric and magnetic fields in the excitation region. The overall decay rates of the excited states can vary by a large amount, owing to the enormous differences between the annihilation and florescence lifetimes of the accessible field-free states. The energy-level structure, spectral intensities, and florescence and annihilation lifetimes in the presence of the fields were determined from the eigenvalues and eigenvectors of the complete $n = 2$ Hamiltonian matrix in an $|nS\ell JM_J\rangle$ basis. Using these data as the input to a Monte Carlo model yielded calculated values which could be compared with experimentally measured quantities; qualitative agreement with the measurements was found. Varying the electric field in the presence of a weak parallel magnetic field provides control over the amount of level mixing that occurs, making it possible to increase or decrease the Ps lifetime. Field-controlled Ps decay can be used as an ionization-free detection method. Conversely, increasing the excited-state lifetime can potentially be exploited to optimize multistep excitation processes using mixed intermediate states. This will be useful either in minimizing losses through intermediate-state decay during excitation or by making it possible to separate excitation laser pulses in time. In addition, the adiabatic extraction of appropriate eigenstates from the electric field in which they are excited can, in principle, be used to prepare pure $2\,^3S_1$ atoms. The availability of atoms in these states produced via single-photon excitation will facilitate high-resolution microwave spectroscopy of the Ps $n = 2$ fine structure.

DOI: 10.1103/PhysRevA.93.012506

I. INTRODUCTION

Positronium (Ps) is a hydrogenic metastable electron-positron bound state [1]. Ps has been studied experimentally for decades [2] in a diverse range of areas [3,4], from probing solid-state materials [5] to fundamental QED tests [6] and searches for physics beyond the standard model [7]. Being composed of a particle-antiparticle pair, Ps is intrinsically metastable due to self-annihilation, but the decay rates are low enough to ensure that Ps has a well defined atomic structure. Although the coarse energy levels of Ps are those of atomic hydrogen scaled by a factor of 1/2, strong spin-spin interactions and virtual annihilation contributions give rise to a Ps substructure that differs significantly from that of hydrogen [8,9]. For example, the energy difference between the singlet and triplet levels of the ground state in Ps is 203 GHz [10], whereas the corresponding splitting in hydrogen is only 1.4 GHz [11].

While virtual annihilation processes affect the fine structure of Ps energy levels, real annihilation events are an important feature in many Ps experiments [12]. This process converts the electron and positron into γ-ray photons [3], which can be used to detect Ps atoms. Time-resolved annihilation measurements can be implemented to perform spectroscopy of Ps (e.g., [13]) because the different energy levels can have significantly different annihilation rates. For instance, the mean lifetimes of the triplet, $1\,^3S_1$ (142 ns), and singlet, $1\,^1S_0$ (125 ps), ground states differ by over three orders of magnitude. Consequently, any mechanism that converts $1\,^3S_1$ atoms into $1\,^1S_0$ atoms will be readily observable in annihilation lifetime spectra [14,15].

Ps annihilation requires overlap of the positron and electron wave functions [16]. Since Ps is described by hydrogenic wave functions, this overlap depends on the square of the radial wave function at the origin and is zero for states with $\ell > 0$ [9]. Therefore, only higher order channels contribute to the annihilation rate of all but S states. These channels are highly suppressed [17], and in practice only the $1\,^1S_0$, $1\,^3S_1$, $2\,^1S_0$, and $2\,^3S_1$ levels can self-annihilate; all other levels decay by fluorescence to one of these before annihilating. The $2\,^1S_0$ and $2\,^3S_1$ levels are metastable (since their primary decay mode is two-photon emission) with fluoresce occurring in $\simeq$0.24 s [18], much longer than their annihilation lifetimes (1 ns and 1.14 μs, respectively). Conversely, the $2\,P_J$ levels fluoresce in 3.19 ns, but have annihilation lifetimes in excess of 100 μs [17,19]. The annihilation and fluorescence lifetimes of $n = 1$ and $n = 2$ states in Ps are summarized in Table I. The inhibition of annihilation for states with $\ell > 0$ and the diverse range of fluorescence and annihilation rates is the basis for several proposed methods to manipulate Ps lifetimes using various laser fields [23–30].

Here we describe in detail recent experiments in which the annihilation dynamics of excited Ps atoms are controlled via combined Stark and Zeeman interactions [31]. Parallel electric and magnetic fields and different photoexcitation laser polarizations were used to control the admixture of states with different orbital angular momentum and spin multiplicity in the $n = 2$ manifold. When the fields were tuned to maximize the amount of $2\,^1P_1$ character of the excited eigenstates, while still maintaining efficient excitation from the $1\,^3S_1$ level, decay to the $1\,^1S_0$ level could occur, leading to rapid annihilation.

TABLE I. Annihilation ($\tau_{\text{ann.}}$) and fluorescence ($\tau_{\text{fl.}}$) lifetimes for the $n = 1$ and $n = 2$ states of Ps.

Level	$\tau_{\text{ann.}}$ (ns)	Ref.	$\tau_{\text{fl.}}$ (ns)	Ref.
$1\,^1S_0$	0.125	[20]	N/A	N/A
$1\,^3S_1$	142	[21]	$\gtrsim 10^{16}$	[22]
$2\,^1S_0$	1	[20]	$\simeq$243 100 000	[18]
$2\,^3P_0$	100 000	[17]	3.19	[9]
$2\,^3P_1$	$\simeq\infty$	[17]	3.19	[9]
$2\,^1P_1$	3 330 000	[19]	3.19	[9]
$2\,^3P_2$	384 000	[17]	3.19	[9]
$2\,^3S_1$	1 136	[21]	$\simeq$243 100 000	[18]

Similarly, optical excitation to mixed states with $2\,^1S_0$ character may result in direct annihilation from the excited state. Both of these mechanisms can be utilized for Ps detection. On the other hand, increasing the proportion of $2\,^3S_1$ character in excited mixed states can extend their lifetime, which can help optimize subsequent excitation to higher energy levels, either by reducing losses via intermediate-state decay or by facilitating excitation using time-separated excitation laser pulses. In addition, if certain mixed states with a significant $2\,^3S_1$ component are adiabatically extracted from the electric field in which they are produced, ensembles of pure $2\,^3S_1$ atoms may be produced in zero field following single-photon excitation.

II. EXPERIMENTAL METHODS

A. Positron beam and positronium production

The experiments reported here involve the optical excitation of Ps atoms generated following positron accumulation in a Surko-type trap [32]. A detailed description of the apparatus and methods used to achieve this have been given elsewhere [33], and similar experimental arrangements have been reported previously [34,35]. Pulses containing $\sim 10^5$ positrons are emitted from the trap every second and are time bunched [36] to 4 ns duration [full width at half maximum (FWHM)]. The positrons are accelerated to 2.2 keV and implanted into a porous silica film [37–39], from which Ps atoms are subsequently emitted into vacuum with near-thermal energies [35,40]. We use these Ps formation targets because they are efficient, robust, and stable, requiring no special preparation or maintenance after installation in the vacuum system. Once created in the bulk material, Ps is emitted from the target in a few nanoseconds [41], resulting in the creation of a dilute Ps gas near the silica surface with an initial number density of the order of 10^7 cm^{-3}.

The porous silica target was mounted between two parallel electrodes, as shown in Fig. 1(a). The positron beam passed through a tungsten grid, in one of the electrodes, with a geometrical transmission of approximately 70%. By applying appropriate potentials to the grid and target electrodes [see Fig. 1(b)], the electric field in the Ps excitation region could be controlled without affecting the positron implantation energy. For the experiments reported here this was fixed at 2.2 keV, chosen to simultaneously optimize the Ps yield and energy [41]. As a result the incident positron beam interacts with the grid at different energies, depending on the desired electric

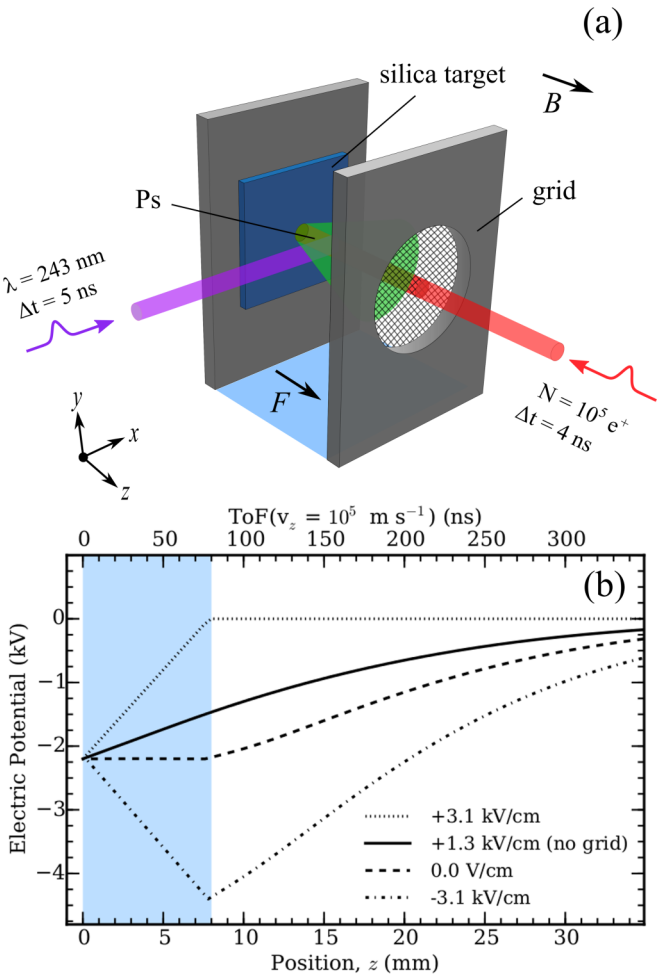

FIG. 1. (a) Schematic diagram of the Ps formation and laser interaction region. The green cone emanating from the porous silica represents Ps formed by implanting positrons into the film. (b) Calculated electric potentials in the target region, the legend indicates the magnitude and direction of the electric field in the area between the target and the grid indicated by the (blue) shaded region. The flight time for Ps with a velocity of $v_z = 10^5$ ms^{-1} is shown on the top axis.

field. When the potential applied to the grid is high, positron-grid collisions result in positrons that become trapped in the (untreated) bulk material, where they annihilate. However, at lower impact energies positrons will be more likely to return to the surface region, where Ps formation is possible [42].

Measurements of Ps formation in the porous silica target for different electric fields exhibit an asymmetric dependence on the direction of the field, owing to the grid-potential-dependent Ps formation mechanism, shown in Fig. 2. These data indicate the amount of Ps formed (quantified by f, defined in Sec. II B) for different electric fields and for the corresponding grid potential. Ps formation on the grid is suppressed at high implantation energies since the diffusion length of positrons in materials with many defects is low [43,44]. The Ps formed on the grid does not interact with the laser and therefore does not affect our Ps excitation measurements, as is demonstrated in Sec. IV. We note that this effect can be minimized by using finer grid material, through which $> 90\%$ transmission is achievable.

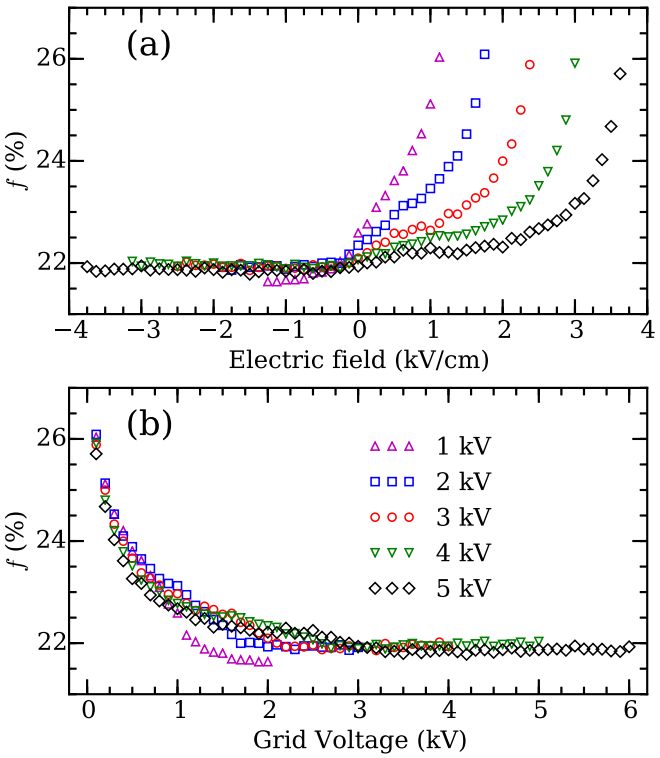

FIG. 2. (a) Measurements of f as a function of the electric field in the interaction region. The measurements were performed for five different target voltages (which define the positron pulse implantation energy) and the field was modified by changing the voltage applied to the grid [see Fig. 1(a)]). Panel (b) is as panel (a) but displayed as a function of the applied grid voltage, showing that the increase in f for high positive electric fields is due to grid-formed Ps alone. The error bars are smaller than the symbols in both plots.

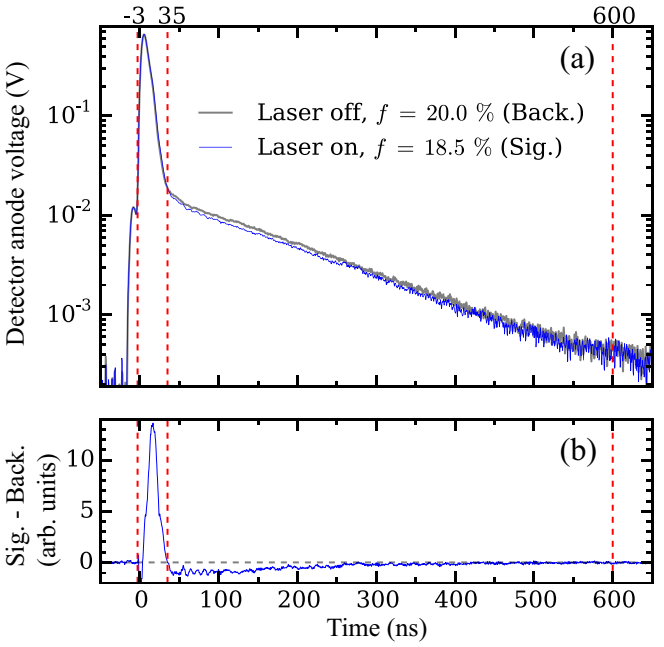

FIG. 3. (a) Example of SSPALS lifetime spectra recorded with the UV laser off resonance (continuous gray line) and on resonance (continuous blue line). (b) Subtraction of background data from signal. These spectra were recorded at a magnetic field of $B = 130$ G and an electric field of $F = 585$ V/cm. Each set of data is the average of 180 pulses. Shown as vertical red dashed lines are the positions of the time windows A (−3 ns), B (35 ns), and C (600 ns).

B. γ-ray detection

The number of γ-ray photons (N) emitted by the self-annihilation of a Ps atom is dictated by charge conjugation invariance through the selection rule [45–47]

$$(-1)^{\ell+S} = (-1)^N. \tag{1}$$

Here ℓ and S are the orbital angular momentum and spin of the Ps atom, respectively. According to Eq. (1), $1\,^1S_0$ ($1\,^3S_1$) atoms must decay into an even (odd) number of γ rays. For free atoms, radiationless [48] and single-photon [49] decay are suppressed by energy and momentum conservation requirements. Thus, two- and three-photon emission are the dominant Ps decay modes. Self-annihilation of singlet ground-state Ps will result in the emission two anticollinear 511-keV γ rays, whereas triplet Ps atoms decay predominantly via the emission of three photons of lower energy [21,50]. This distinction is the principle reason for the large difference between the decay rates of singlet and triplet Ps atoms [4]. Consequently, either energy or time-resolved γ-ray spectroscopy can be used to identify the production of triplet Ps atoms [2]. In this work we use time-resolved measurements; in principle, one could perform energy-resolved γ-ray spectroscopy with intense positron pulses [51], but the efficacy of doing so has not yet been demonstrated.

Positron annihilation lifetime spectroscopy (PALS) is a well-known technique in positron physics in which single annihilation events are detected using fast γ-ray detectors [52,53] to avoid detector pileup (e.g., [54]). In the experiments we describe here, and more generally in the Ps optical excitation work [6], many Ps atoms are created simultaneously, which precludes using conventional PALS detection methods unless the detector acceptances are severely restricted [55].

In order to utilize as many annihilation photons per pulse as possible, we instead employ single-shot positron annihilation lifetime spectroscopy (SSPALS) [56]. Here a fast detector is coupled to an oscilloscope and $V(t)$, the time-dependent detector anode voltage, is measured directly. This signal is proportional to the annihilation radiation flux, and the resulting waveform constitutes a lifetime spectrum. Examples of such spectra are shown in Fig. 3. In the present work on the order of 10^6 γ rays result from each positron pulse, approximately 5% of which are subsequently detected in a time window that is typically less than 10 ns wide. The detector used was a lead tungstate ($PbWO_4$) scintillator, optically coupled to a photomultiplier tube [57]. The SSPALS time resolution is determined primarily by the ∼12-ns scintillator decay time, which is sufficient to study processes that occur on the ∼100 ns time scale associated with the decay of $1\,^3S_1$ Ps atoms.

The SSPALS signal is parametrized by f, the fraction of the lifetime spectrum in a selected time region where

$$f = \int_B^C V(t)dt \Big/ \int_A^C V(t)dt. \tag{2}$$

The time regions are selected depending on the experimental parameters; here we wish to study laser-induced changes in Ps lifetimes that occur on a short time scale relative to the typical decay rate of the $1\,^3S_1$ ground state ($1/142$ ns $= 7$ MHz). Accordingly, the time windows used were $A = -3$ ns, $B = 35$ ns, and $C = 600$ ns (see Fig. 3). Note that while the actual value of f depends on the choice of the time windows, and is therefore arbitrary, for certain configurations it depends almost linearly on the positronium formation fraction, as discussed in Ref. [58].

We characterize laser-induced effects on Ps decay rates using the parameter

$$S_\gamma = (f_{\rm bk} - f_{\rm sig})/f_{\rm bk}, \tag{3}$$

where $f_{\rm bk}$ refers to background measurements with no lasers present, and $f_{\rm sig}$ refers to the signal when the laser is on, as shown in Fig. 3. With the experimental parameters described above, if Ps atoms are excited to $2\,^3P_J$ levels in zero field, and subsequently return to the $1\,^3S_1$ level (either via spontaneous or stimulated emission), we would measure $S_\gamma \simeq 0$, because the lifetime spectra are not significantly altered by the small decrease in the total Ps decay rate. However, if annihilation occurs as a result of excitation, either following photoionization or, as we discuss in Sec. IV, through magnetic quenching, then we would measure positive values for S_γ. If atoms are excited to long-lived states, we would observe negative S_γ values.

C. Laser excitation

Ps atoms are excited from the ground state to $n = 2$ levels via $1\,^3S_1 \rightarrow 2\,^3P_J$ transitions using ultraviolet (UV) radiation from a pulsed laser system [33]. Radiation of wavelength 243.01 nm was generated by frequency doubling the 486.02-nm output of a dye laser (operated with Coumarin 102 dye), which was pumped by the third harmonic (355 nm) of a Q-switched Nd:YAG laser. Energies of up to 4 mJ/pulse of UV radiation could be generated, with a duration of 6 ns (FWHM) and a bandwidth of 85 GHz. Typical pulse energies for the experiments we report were ~0.5 mJ in a beam with spatial dimensions of approximately 10 by 5 mm, resulting in fluences sufficient to saturate the $1\,^3S_1 \rightarrow 2\,^3P_J$ transition. For experiments in which photoionization was performed, a second independent Nd:YAG laser (second harmonic, 532 nm) and an infrared (IR) pulsed dye laser (729 nm) were used.

The natural $1\,^3S_1 \rightarrow 2\,^3P_J$ linewidth is ~50 MHz, due to the 3.19-ns $2\,^3P_J$ fluorescence lifetime. However, the Ps atoms have mean speeds of the order of 10^5 m/s. As a result, the observed transitions are Doppler broadened to widths of ~500 GHz [35]. Therefore, the ~20% spectral overlap of the UV laser and the Doppler-broadened $1\,^3S_1 \rightarrow 2\,^3P_J$ transition represents the limiting factor in the efficiency of excited-state production.

In principle, it is possible for the UV laser to excite $1\,^3S_1$ atoms to $n = 2$ states with mixed singlet and triplet character and then to drive transitions back to the $1\,^1S_0$ level. Such transitions would result in a quenching signal that has not been included in our analysis. However, due to the large separation between the $1\,^3S_1$ and $1\,^1S_0$ levels (203 GHz [10]) and the 85-GHz laser bandwidth, the excitation of such a crossover resonance (e.g., [59]) can happen only if the laser is tuned off resonance and retroreflected into the excitation region, such that UV radiation interacts with Ps atoms that have the correct Doppler shifts [60]. For the experiments described here the laser wavelength was set to the resonance frequency (or was completely off resonance at 243.4 nm), and therefore such processes can be neglected. This means that any quenching events in which atoms were transferred to the $1\,^1S_0$ level from the $1\,^3S_1$ level via the $n = 2$ manifold must have occurred via spontaneous decay.

III. CALCULATIONS

To quantify the contributions of the electric and magnetic fields in the experiments to the rates of Ps annihilation, the combined Stark and Zeeman effects for states with $n = 2$ have been calculated. These calculations treated all singlet and triplet terms, and their associated fine structure, and were performed by determining the eigenvalues and eigenvectors of the complete Hamiltonian matrix in an $|nS\ell JM_J\rangle$ basis, following the convention of Bethe and Salpeter [9]. Here n is the principal quantum number, S is the total spin quantum number of the electron-positron pair, ℓ is the single particle orbital angular momentum quantum number, $J = |\vec{J}| = |\vec{\ell} + \vec{S}|$ is the total angular momentum quantum number, and M_J is the projection of $\vec{J}$ onto the z axis with which the applied electric and magnetic fields are aligned. The approach used in these calculations is similar to that implemented previously by Curry [61] and Dermer and Weisheit [62].

In the $n = 1$ ground state of Ps, the energy interval between the singlet and triplet terms is $E_{\rm hfs}(n = 1)/h = 203.3942$ GHz [63] (see Fig. 4). Because the magnitude of the spin-spin interactions, which give rise to this energy splitting, depends on the overlap of the electron and positron wave functions, for values of $n > 1$ the energy splittings reduce, scaling with n^{-3} [64]. For $n = 2$, the energy intervals between the singlet and triplet terms are indicated in Fig. 4. The fine-structure splittings between each of the $2\,^3P_J$ levels are also indicated in this figure.

A. Calculation methods

In the presence of parallel electric and magnetic fields, the Hamiltonian, $\hat{H}$, for Ps atoms can be expressed in the form

$$\hat{H} = \hat{H}_0 + \hat{H}_{\rm Z} + \hat{H}_{\rm S}, \tag{4}$$

where $\hat{H}_0$ represents the unperturbed Hamiltonian including the fine-structure contributions; $\hat{H}_{\rm Z} = -\vec{\mu}_{\rm mag} \cdot \vec{B}$ is the Zeeman Hamiltonian arising from the presence of a magnetic field $\vec{B}$, where $\vec{\mu}_{\rm mag} = \vec{\mu}_{\rm e^-} + \vec{\mu}_{\rm e^+}$ is the combined magnetic moment of the electron-positron pair; and $\hat{H}_{\rm S} = -e\vec{F} \cdot \vec{r}$ is the Stark Hamiltonian resulting from the interaction with an external electric field $\vec{F}$, where e is the electron charge and $\vec{r}$ is the position vector.

To express $\hat{H}$ in matrix form for levels with $n = 2$, we consider a 16×16 matrix in an $|nS\ell JM_J\rangle$ basis. Because of the comparatively weak fields used in the experiments described here, only $n = 2$ levels need be considered in this basis. The 16 basis states therefore represent the individual M_J sublevels associated with each level in the upper part of Fig. 4. In this basis, $\hat{H}_0$ is a diagonal matrix and the energies of the diagonal elements are those in Fig. 4.

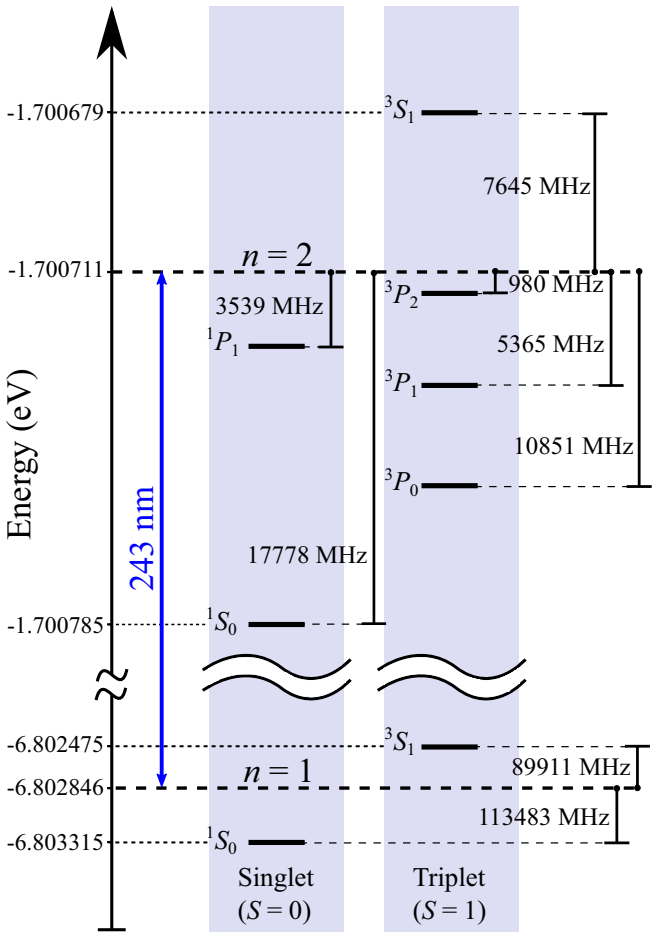

FIG. 4. Ps energy-level diagram indicating the fine structure of states with $n = 1$ and $n = 2$. The intervals between each level are denoted by their relative frequency with respect to the energies given by the Rydberg formula $E(n) = -6.8\ \mathrm{eV}/n^2$.

For a magnetic field $\vec{B} = (0,0,B)$ acting in the z direction, the Zeeman Hamiltonian takes the form

$$\hat{H}_{\mathrm{Z}} = g_{\mathrm{e}}\mu_{\mathrm{B}}\hat{s}_{z_{e^-}}B - g_{\mathrm{e}}\mu_{\mathrm{B}}\hat{s}_{z_{e^+}}B, \tag{5}$$

where $\hat{s}_{z_{e^-}}$ ($\hat{s}_{z_{e^+}}$) is the projection operator of the electron (positron) spin onto the z axis, g_{e} is the electron ($\equiv$ positron) spin g factor, and μ_{B} is the Bohr magneton. Because of the equal masses of the electron and the positron, the magnetic moment associated with the net orbital angular momentum in Ps is zero. Therefore, the Zeeman interaction is independent of $\vec{\ell}$ [61]. The matrix corresponding to Eq. (5) contains off-diagonal elements coupling sublevels with equal values of ℓ and M_J, and values of S that differ by ± 1, i.e., the magnetic-field couples singlet and triplet terms. The matrix elements between sublevels $|nS\ell JM_J\rangle$ and $|nS'\ell'J'M'_J\rangle$ can be expressed as [62]

$$\begin{aligned}&\langle nS'\ell'J'M'_J|\hat{H}_{\mathrm{Z}}|nS\ell JM_J\rangle \\ &= \mu_{\mathrm{B}}B\,\delta_{\ell',\ell}(-1)^{\ell+M_J}[(-1)^{S+S'}-1]\sqrt{3(2J'+1)(2J+1)} \\ &\quad\times\begin{pmatrix} J' & 1 & J \\ -M'_J & 0 & M_J\end{pmatrix}\begin{Bmatrix} S' & \ell' & J' \\ J & 1 & S\end{Bmatrix},\end{aligned} \tag{6}$$

where $\delta_{x,x'}$ is the Dirac δ function, and the term in curved (curly) brackets is a Wigner $3J$ ($6J$) symbol.

In an electric field $\vec{F} = (0,0,F)$ aligned parallel to the magnetic field, the Stark Hamiltonian contains off-diagonal elements coupling sublevels with equal values of S and M_J and values of ℓ that differ by ± 1. The matrix elements between pairs of sublevels take the form [62]

$$\begin{aligned}&\langle nS'\ell'J'M'_J|\hat{H}_{\mathrm{S}}|nS\ell JM_J\rangle \\ &= eF\,\delta_{S',S}(-1)^{S+1+M'_J}\sqrt{\ell_{\max}(2J'+1)(2J+1)} \\ &\quad\times\begin{pmatrix} J' & 1 & J \\ -M'_J & 0 & M_J\end{pmatrix}\begin{Bmatrix} S' & \ell' & J' \\ 1 & J & \ell\end{Bmatrix}\langle n'\ell'|r|n\ell\rangle,\end{aligned} \tag{7}$$

where $\ell_{\max} = \max(\ell',\ell)$ and $\langle n'\ell'|r|n\ell\rangle$ is a radial integral. For $n = 2$ and $|\ell' - \ell| = 1$, $|\langle n'\ell'|r|n\ell\rangle| = 3\sqrt{3}a_{\mathrm{Ps}}$, where $a_{\mathrm{Ps}} = 2a_0$ is the Ps Bohr radius.

Combining the Zeeman and Stark matrices with the diagonal zero-field matrix allows the $n = 2$ energy-level structure to be determined in parallel fields of all magnitudes relevant to the experiments described here. This is achieved by calculating the set of eigenvalues, E_i, labeled with the index i, of the complete Hamiltonian matrix for each field strength of interest. Spectral intensities and decay rates can then be obtained from the coefficients, $C_{i,j}$, of the corresponding eigenvectors, where j is an index denoting each $|nS\ell JM_J\rangle$ basis state.

Under the electric dipole selection rules, optical transitions from the $1\,^3S_1$ and $1\,^1S_0$ levels of the ground state to excited $n = 2$ states occur only if $\Delta S = 0$, $\Delta\ell = \pm 1$ and $\Delta J = 0,\pm 1$ ($0 \not\leftrightarrow 0$) [9]. In photoexcitation the values of M_J of the excited sublevels can be controlled by adjusting the polarization of the laser radiation with respect to the electric and magnetic fields. For laser radiation propagating perpendicular to both fields, as in the experiments, if it is linearly polarized parallel to the axis defined by the fields (z axis), $\Delta M_J = 0$ transitions will result [see, e.g., Fig. 5(a)], whereas if it is linearly polarized perpendicular to this axis, $\Delta M_J = \pm 1$ transitions will result [see, e.g., Fig. 5(b)]. The resulting transitions between states $|nS\ell JM_J\rangle$ and $|n'S'\ell'J'M'_J\rangle$ have transition dipole moments, $M_{n'S'\ell'J'M'_J,nS\ell JM_J}$,

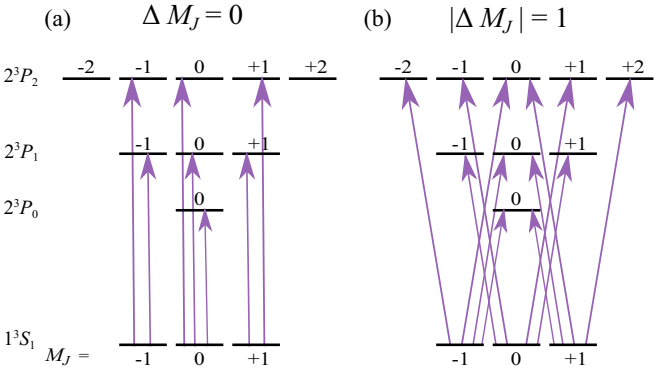

FIG. 5. Allowed electric dipole transitions from each $1\,^3S_1$ sublevel of Ps to all $2\,^3P_J$ sublevels, for laser radiation linearly polarized (a) parallel ($\Delta M_J = 0$) and (b) perpendicular ($|\Delta M_J| = 1$) to the laboratory-fixed quantization axis.

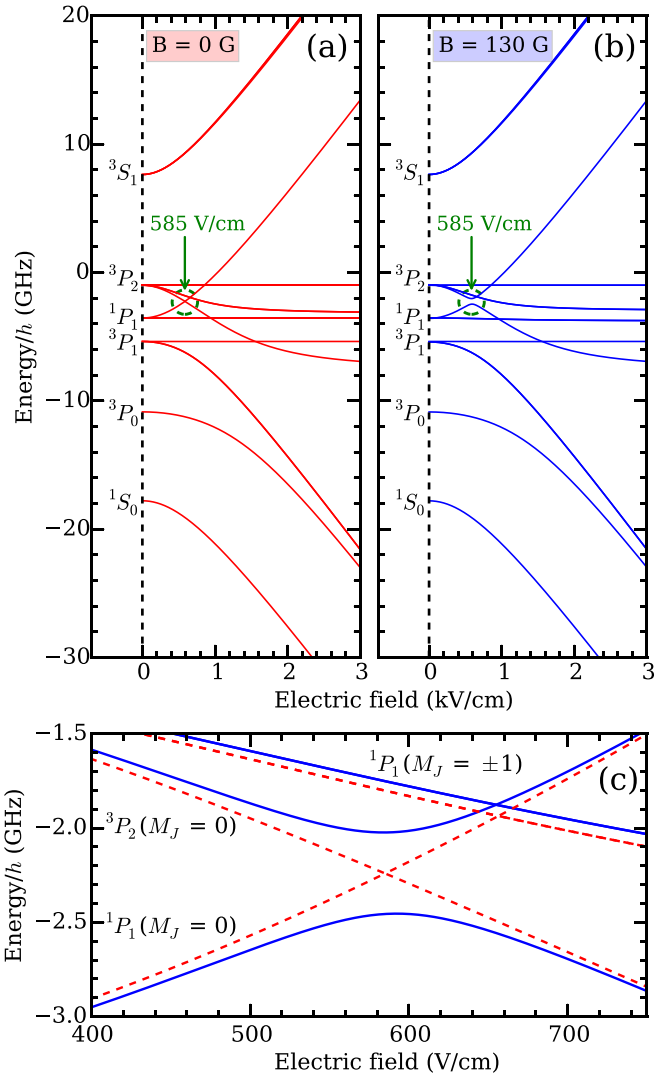

FIG. 6. Dependence of the relative energies of all $n = 2$ eigenstates in Ps on electric-field strength (a) in the absence of a magnetic field and (b) in a parallel magnetic field of $B = 130$ G. (c) An expanded view of the regions enclosed by the dashed circles in (a) and (b). The results of calculations performed for $B = 0$ G (dashed red curves) and $B = 130$ G (continuous blue curves) are presented.

such that

$$M_{n'S'\ell'J'M'_J,nS\ell JM_J} = (-1)^{J-M_J}\sqrt{(2J+1)(2J'+1)} \times \begin{pmatrix} J & 1 & J' \\ -M_J & \Delta M_J & M'_J \end{pmatrix} \times \begin{Bmatrix} \ell & J & S' \\ J' & \ell' & 1 \end{Bmatrix} \langle 2\ell'|er|1s\rangle. \quad (8)$$

B. Calculated $n = 2$ energy-level structure

A Stark energy-level diagram, calculated for the $n = 2$ states of Ps in electric fields up to 3 kV/cm when $B = 0$ G, is displayed in Fig. 6(a). In fields below 1 kV/cm in this figure, the S and P terms of each spin multiplicity exhibit quadratic Stark energy shifts as they gradually mix with each other. In higher fields, linear Stark shifts dominate when the interaction with the electric field becomes greater than the spin-spin and spin-orbit interactions. In all of the experiments reported here a magnetic field, $B = 130$ G, was present at the position of Ps photoexcitation (unless stated otherwise). The effect of this magnetic field, which was oriented parallel to the electric field, on the $n = 2$ Stark energy-level structure can be seen in Fig. 6(b).

Comparing Figs. 6(a) and 6(b) shows that the weak magnetic field of 130 G does not significantly affect the overall Stark structure. However, there is one particular point in the Stark map, indicated by the dashed circles in Figs. 6(a) and 6(b), where the singlet-triplet mixing induced by the magnetic field has a noticeable effect. In this electric field of 585 V/cm, the energy-level crossing between the outermost $2\,^1P_1$ sublevel with a positive Stark energy shift (i.e., that for which $M_J = 0$) and the outermost $2\,^3P_2$ sublevel with a negative Stark energy shift (also with $M_J = 0$) changes from an exact crossing to an avoided crossing as a result of the coupling between the sublevels induced by the magnetic field. An expanded view of this region of the Stark map can be seen in Fig. 6(c). When $B = 130$ G, at the avoided crossing the wave functions of the two interacting sublevels contain approximately equal amounts of $2\,^3P_2\,(M_J = 0)$ character and $2\,^1P_1\,(M_J = 0)$ character [31]. These mixed states can therefore be efficiently photoexcited from the $1\,^3S_1$ level, but once populated have a high probability, ~0.5, of decaying to the $1\,^1S_0$ level, which can subsequently rapidly self-annihilate. Consequently, strong singlet-triplet mixing of this kind in combined electric and magnetic fields can be exploited to transform a sample of triplet Ps atoms into short-lived singlet atoms via photoexcitation to states with $n = 2$.

C. Excited-state decay rates

To obtain more detailed information on the rates of decay of the excited $n = 2$ eigenstates in the presence of the combined electric and magnetic fields, the fluorescence and annihilation rates of Ps atoms initially prepared in the $1\,^3S_1$ level and subsequently photoexcited via electric dipole allowed $1\,^3S_1 \rightarrow 2\,^3P_J$ single-photon transitions have been calculated. This was done by first determining the rates for fluorescence, $\Gamma_{\rm fl}$, and direct annihilation, $\Gamma_{\rm ann}$, of each $n = 2$ sublevel in the presence of the fields, using the data in Table I, together with the coefficients of the eigenvectors, $C_{i,j}$, of the Hamiltonian matrix, such that

$$\Gamma_{{\rm fl},i} = \sum_j C_{i,j}^2\,\Gamma_{{\rm fl},j} \quad (9)$$

and

$$\Gamma_{{\rm ann},i} = \sum_j C_{i,j}^2\,\Gamma_{{\rm ann},j}. \quad (10)$$

Following this procedure, the total lifetime, $\tau_{{\rm tot},i}$, of each eigenstate could be determined,

$$\tau_{{\rm tot},i} = (\Gamma_{{\rm fl},i} + \Gamma_{{\rm ann},i})^{-1}. \quad (11)$$

These calculated excited-state lifetimes are displayed in Figs. 7(a) and 7(b) for cases in which $B = 0$ G and $B = 130$ G, respectively. From these data it can be seen in both cases that,

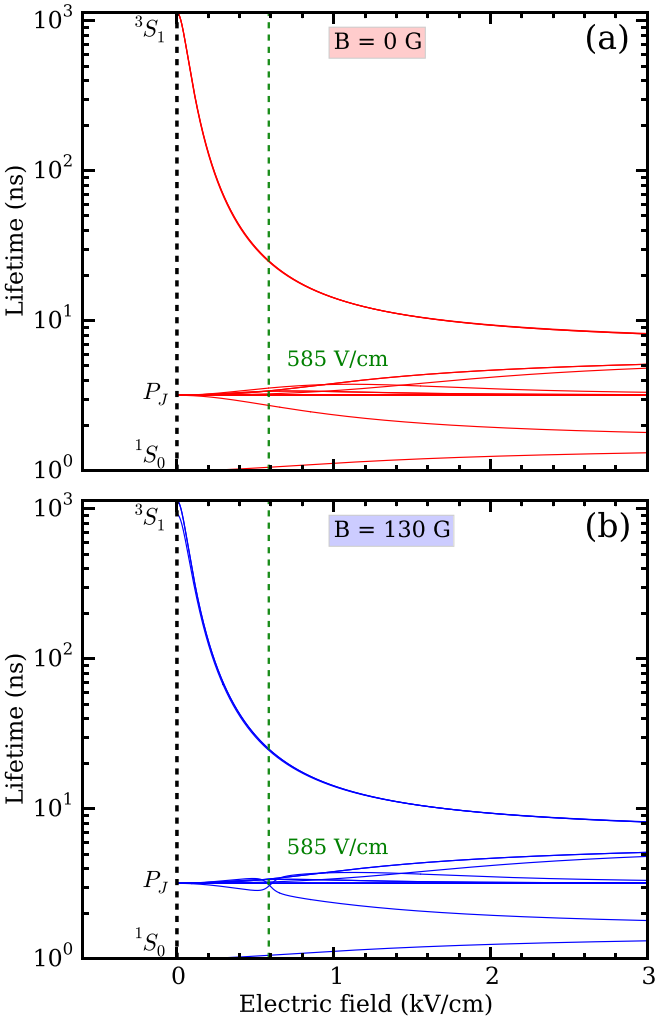

FIG. 7. Dependence of the combined fluorescence and annihilation lifetimes of the $n = 2$ eigenstates in Ps on electric-field strength for (a) $B = 0$ G and (b) $B = 130$ G. The term symbols associated with the field-free eigenstates are indicated on the left side of each panel.

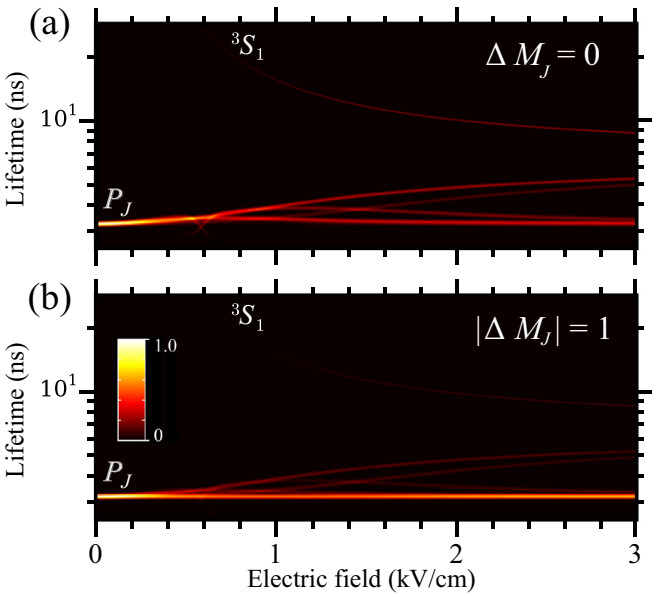

FIG. 8. The electric-field dependence of the total lifetimes (in the range from 2.5 to 25 ns) of the $n = 2$ eigenstates accessible by single-photon excitation from the $1\,^3S_1$ level when $B = 130$ G [as in Fig. 7(b)]. The color scale represents the relative strength of the electric dipole transitions for laser radiation linearly polarized (a) parallel ($\Delta M_J = 0$) and (b) perpendicular ($|\Delta M_J| = 1$) to the z axis, with which the electric and magnetic fields are aligned.

as the strength of the electric field increases, mixing of the S and P terms leads to a reduction in the total lifetimes of the Stark states that adiabatically evolve, from high to low electric field, to the $2\,^3S_1$ level. The lifetimes of these states reduce from 1 μs when $F = 0$ V/cm to <10 ns when $F \gtrsim 1$ kV/cm. On the other hand, the lifetime of the short-lived $2\,^1S_0$ level, which decays predominantly by direct annihilation, increases slightly with increasing electric field.

In the presence of an electric field, the lifetimes of the $2\,P$ states evolve in three ways: (1) The total lifetimes of the $2\,^3P_J$ levels that mix with the $2\,^3S_1$ level increase; (2) levels which remain unmixed in the field, i.e., those for which $|M_J| = 2$, maintain their field-free 3.19-ns lifetime; and (3) the lifetimes of the levels that mix with the $2\,^1S_0$ level [e.g., the $2\,^1P_1$ ($M_J = 0$)], are reduced, in this case from 3.19 ns when $F = 0$ V/cm to ~2 ns when $F = 3$ kV/cm.

The effect of singlet-triplet mixing, induced by the presence of the magnetic field of $B = 130$ G, on the lifetimes of each of the Stark eigenstates can be seen in Fig. 7(b). The principal difference between this case and that in Fig. 7(a) is seen close to $F = 585$ V/cm, the field at which the avoided crossing in Fig. 6(c) occurs. In this field, the slightly reduced lifetime of the $2\,^1P_1(M_J = 0)$ sublevel that arises when it mixes with the $2\,^1S_0$ level in the electric field, causes a subsequent reduction in the lifetime of the $2\,^3P_2(M_J = 0)$ sublevel with which it interacts when the magnetic field is present. This indicates that, although the primary effect of the magnetic field in this region of the Stark map is to permit decay by fluorescence of states with $2\,^3P_J$ character to the short-lived $1\,^1S_0$ ground-state followed by rapid self-annihilation, there is also a small contribution from direct annihilation at $n = 2$.

In the experiments described here ensembles of Ps atoms, initially in the $1\,^3S_1$ level, were excited via single-photon transitions to $n = 2$ eigenstates with ^3P_J character. As a result, the excited-state lifetimes of importance are those of the states which are accessible via this photoexcitation scheme. The lifetimes of these states can be identified in Fig. 8. The electric-field dependence of the lifetimes of the $n = 2$ eigenstates included in this figure are identical to those in Fig. 7(b), while the color scale represents the relative $1\,^3S_1 \rightarrow 2\,^3P_J$ transition dipole moment to each state, calculated using Eq. (8). From these data it can be seen that for $\Delta M_J = 0$ transitions, driven with laser radiation polarized parallel to the axis defined by the electric and magnetic fields [Fig. 8(a)], a slight reduction in the total lifetime of some of the accessible $n = 2$ eigenstates from their field-free values of 3.19 ns occurs in an electric field of 585 V/cm, as a result of mixing with states possessing $2\,^1S_0$ components. However, in higher fields, transitions to longer-lived states with partial $2\,^3S_1$ character also play an important role. For $|\Delta M_J| = 1$ transitions, driven with laser

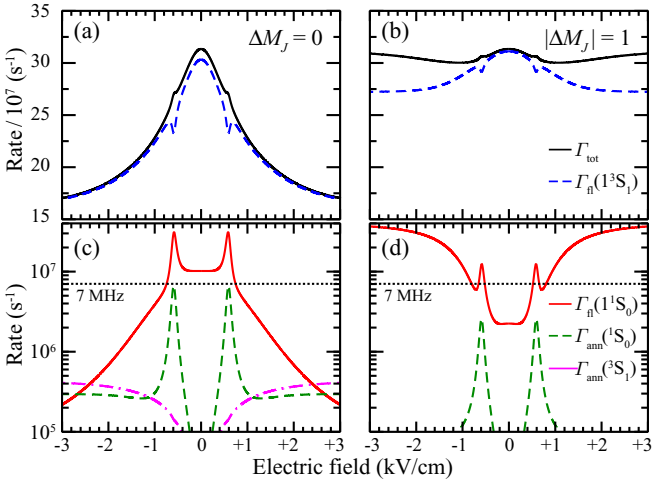

FIG. 9. Spectral-intensity-weighted average $n = 2$ decay rates when $B = 130$ G for photoexcitation via (a),(c) $\Delta M_J = 0$ and (b),(d) $|\Delta M_J| = 1$ transitions from the $1\,^3S_1$ level. (a),(b) Total $n = 2$ decay rates, Γ_{tot}, (continuous black curve), and triplet fluorescence rate, $\Gamma_{fl}(1\,^3S_1)$, (dashed blue curve). (c),(d), fluorescence rate to the $1\,^1S_0$ level, $\Gamma_{fl}(1\,^1S_0)$ (continuous red curve), and direct $2\,^1S_0$, $\Gamma_{ann}(^1S_0)$ (dashed green curve), and $2\,^3S_1$, $\Gamma_{ann}(^3S_1)$ (dash-dotted magenta curve) annihilation rates. The horizontal dashed lines in (c) and (d) correspond to the 7 MHz annihilation rate of the $1\,^3S_1$ level.

radiation polarized perpendicular to the fields, only a very slight change in the direct $n = 2$ decay rates occurs in weak electric fields, while in strong fields the accessible sublevels to which the strongest transitions occur do not exhibit lifetimes significantly longer than those of the field-free levels.

The dependence of the total lifetimes of the $n = 2$ eigenstates on the electric and magnetic fields displayed in Figs. 7 and 8 does not, however, provide a complete picture of Ps annihilation in the experiments. The dominant contribution to this results from spontaneous emission from excited states with $2\,^1P_1$ character to the $1\,^1S_0$ level, which rapidly self-annihilates. To identify the role of this process and its significance when compared to the other possible Ps decay pathways, spectral-intensity-weighted average decay rates were determined for each electric–field strength considered in the experiments. These average decay rates, presented in Fig. 9, were calculated by assuming an equal laser intensity across the frequency range encompassed by the manifold of $n = 2$ levels in the presence of the fields. Displayed in Figs. 9(a) and 9(b) are weighted-average total decay rates calculated for each laser polarization from the values of $\Gamma_{fl,i}$ and $\Gamma_{ann,i}$ [see Eqs. (9) and (10)] and the squares of the corresponding transition dipole moments, $M_{i,nS\ell JM_J}$, where

$$M_{i,nS\ell JM_J} = \sum_j C_{i,j}^2\, M_{j,nS\ell JM_J}, \tag{12}$$

and $|nS\ell JM_J\rangle$ are the sublevels of the $1\,^3S_1$ ground state. By comparison with the weighted-average values of the fluorescence rate to the $1\,^3S_1$ level, $\Gamma_{fl}(1\,^3S_1)$, also included in these figures, these data indicate that for both laser polarizations the decay of the accessible excited states is dominated, in all electric fields considered, by the contribution from fluorescence via this decay pathway. However, as can be seen in Figs. 9(c) and 9(d), for particular combinations of electric–field strength and laser polarization, decay by fluorescence to the $1\,^1S_0$ is also of importance. This is particularly apparent in a field of 585 V/cm [see Fig. 9(c)] and in fields exceeding 1 kV/cm when the laser polarization is selected to drive $\Delta M_J = \pm 1$ transitions.

D. Monte Carlo model of Ps annihilation

Although the results of the calculations presented in Fig. 9 account for the relative population of each $n = 2$ eigenstate by considering the spectral intensities of the single-photon transitions from the $1\,^3S_1$ level, they do not represent directly the observable quantities in the experiments. The measured values of S_γ [see Eq. (3)] are obtained by integrating the γ-ray signal recorded following Ps annihilation in selected time intervals. To calculate the expected values of S_γ arising from the decay of Ps atoms after photoexcitation to $n = 2$ eigenstates in the combined electric and magnetic fields, a Monte Carlo model was implemented in which each decay pathway was included.

In this calculation initial ensembles of 2×10^5 Ps atoms in the $1\,^3S_1$ level were generated at time $t = 0$. The characteristic 7-MHz annihilation rate, corresponding to the 142-ns self-annihilation lifetime of the $1\,^3S_1$ level, was assigned to these atoms. The probability of the self-annihilation of each atom in the simulation was then assessed using Monte Carlo methods in time intervals of 1 ns. Upon annihilation the corresponding atoms were removed from the simulation. After a delay of 20 ns, to account for the emission of the Ps atoms from the porous silica target and their flight to the position of laser photoexcitation, half of the remaining atoms were defined as being excited via the allowed electric dipole transitions to the eigenstates possessing $2\,^3P_J$ character. This assumed saturation of the photoexcitation process.

The decay pathways of the complete ensemble of atoms were then tracked. Four decay pathways from the excited states were considered: (1) decay by fluorescence to the $1\,^3S_1$ level, (2) decay by fluorescence to the $1\,^1S_0$ level, (3) slow annihilation at $n = 2$ arising from mixing with the $2\,^3S_1$ level, and (4) the more rapid annihilation arising from mixing with the $2\,^1S_0$ level. In each time interval the possibility for each of these processes occurring was assessed for the excited atoms. If a particular atom was considered to annihilate directly, or decay to the $1\,^1S_0$ level, where it would rapidly annihilate, it was counted and removed from the simulation. On the other hand, if an atom was considered to decay by fluorescence to the $1\,^3S_1$ level it remained in the simulation but its annihilation rate was reset to 7 MHz. For each annihilation event one γ ray was considered to be registered by the detector so that after calculating the evolution of the ensemble of atoms for ~ 1 μs a simulated Ps decay curve (similar to those displayed in Fig. 3) was obtained. In each electric field for which the calculation was performed this simulated decay curve was then integrated within the appropriate time windows and a value of S_γ determined. Because the intense γ-ray signal, resulting from Ps annihilation within the silica target at times close to $t = 0$ in the experiments (see Fig. 3), was not accounted for directly in the simulation, it was included as a constant, added

to the integrals associated with the early annihilation-time windows when calculating S_γ. This constant was determined by equating the calculated value of $f_{\rm bk}$ with that determined experimentally. In addition, the detector time response was accounted for by convolution with a response function with a time constant of 12 ns. This approach to calculating S_γ permitted the link to be made between the experimentally recorded data and the Ps annihilation rates.

IV. RESULTS AND DISCUSSION

A. Stark enhancement of magnetic quenching

The principal result of the present study is the controlled mixing of short-lived and long-lived $n = 2$ levels of Ps using magnetic and electric fields. Single-shot lifetime spectra, and also f values, were recorded with the $1\,^3S_1 \rightarrow 2\,^3P_J$ excitation laser on ($\lambda_{\rm UV} = 243.01$ nm) and off ($\lambda_{\rm UV} = 243.40$ nm) resonance for different electric fields and laser polarizations. The value of S_γ [see Eq. (3)] was determined for each electric field, as shown in Fig. 10. All data were recorded in a constant magnetic field of $B = 130$ G, unless otherwise specified. Because S_γ is sensitive only to laser-induced changes in the Ps lifetime spectra, it is not affected by the asymmetry in f due to Ps formation on the grid (discussed in Sec. II A).

The structures observed in these data are in qualitative agreement with the calculated effects of the Stark and Zeeman interactions discussed in Sec. III. The general dependence of the measured and calculated S_γ values on the electric field and laser polarizations are similar, indicating that the underlying physical processes are correctly interpreted. In particular, the peaks at 585 V/cm are clearly due to the mixing between singlet and triplet levels at the avoided crossing [see Fig. 4(c)]. Conversely, the negative S_γ values correspond to the increased lifetime due to the $2\,^3S_1$ level mixing with the $2\,^3P_J$ levels. We note that the positions of the Stark-tuned intensity maxima at 585 V/cm in the experimental data are not exactly symmetric, with the negative-field peak shifted slightly. This may be due to the presence of secondary electrons generated by the positron pulse [65] or the production of photoelectrons by the UV laser [66], which could distort the field in the interaction region.

Since the calculated f values are scaled to match the measured values, the calculated S_γ amplitudes should also match; the fact that they do not suggests that there are additional mechanisms that have not been completely accounted for in our simple Monte Carlo model. These may be related to optical pumping processes that allow more efficient transfer of Ps atoms into states that can annihilate.

As explained in Sec. II B, positive values of S_γ indicate an increased annihilation rate induced by the laser. This occurs when an excited mixed state can directly annihilate due to an admixture of the $2\,^1S_0$ level, or the possibility to fluoresce back to the singlet ground state. As these mechanisms are fundamentally mediated by the Zeeman effect, we refer to them generally as magnetic quenching. Magnetic quenching rates may be substantially increased by additional Stark mixing. In low magnetic fields ($B \simeq 100$ G) this is achieved most effectively when the $2\,^1P_1(M_J = 0)$ sublevel mixes with the $2\,^3P_2(M_J = 0)$ sublevel (see Fig. 7). The resulting atoms will have some singlet character and can therefore decay to the short-lived $1\,^1S_0$ level, effectively reducing the annihilation lifetime. However, to optimize this process, it is not enough to maximize the amount of $2\,^1P_1(M_J = 0)$ character of the excited state, as this would greatly decrease the probability of optically exciting these states in the first place (since ΔS must be 0 in an allowed electric dipole transition). Therefore, the

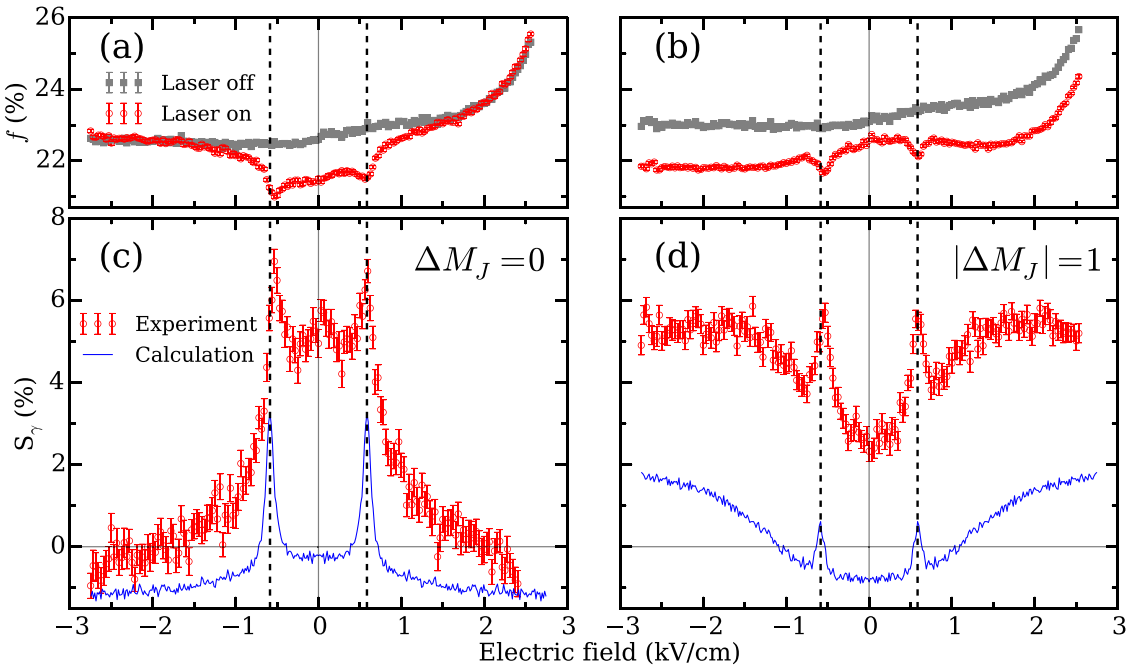

FIG. 10. Measurements of the delayed fraction (f) of the annihilation signal with (red circles) and without (gray squares) the laser radiation present as a function of the applied electric field, for laser radiation polarized linearly (a) parallel and (b) perpendicular to the z axis. The corresponding values of S_γ are shown in (c) and (d), superposed with results of the Monte Carlo simulations (continuous blue lines).

best way to enhance magnetic quenching using Stark mixing is to employ fields that mix $2\,^1P_1(M_J = 0)$ and $2\,^3P_2(M_J = 0)$ levels approximately evenly. In this way, the transition remains strong and there is enough $2\,^1P_1(M_J = 0)$ character to ensure a high probability of fluorescence to the singlet ground state.

In some cases longer-lived $2\,^3S_1$ components may be mixed with the $2\,^3P_J$ states, leading to an increase in their lifetime. By selecting the polarization of the laser radiation to be parallel to the electric field (see Fig. 8), excitation to states with a significant $2\,^3S_1$ component can be optimized. The experimental data together with the results of the calculations shown in Fig. 8 indicate that when the laser radiation is polarized parallel to the magnetic field, the probability of exciting states possessing $2\,^3S_1$ character is increased in high electric fields, leading to negative values of S_γ.

B. Magnetic-field dependence

The reduction of Ps lifetimes due to singlet-triplet mixing in magnetic fields has been observed many times in the ground state [10,15,67] and also in excited states [14,35,68], but the effects of electric fields on Ps level mixing have not been observed before. In the ground state relatively large magnetic fields must be applied (∼1 kG) to obtain significant mixing between the singlet and the triplet levels. As the energy spacing scales approximately with $1/n^3$ [8], the fields required at $n = 2$ in Ps are considerably lower (∼100 G). Nevertheless, the optimal fields for ($n = 2$) magnetic quenching with zero applied electric field are somewhat higher than is sometimes experimentally desirable.

In general, it is much more convenient to use a low magnetic field and increase the quenching rate using electric fields than it is to produce a 1-kG magnetic field. Moreover, electric fields can more easily be pulsed on or off, which may be useful in field-free spectroscopic studies (e.g., [31]). The application of a 130-G magnetic field does not generate a large shift in the energies of the $n = 2$ sublevels (see Fig. 6). However, it does provide sufficient coupling between singlet and triplet levels to facilitate increased magnetic quenching when electric fields are applied. Figure 11 shows results from calculations of the expected fluorescence rate to the short-lived ground state when $F = 0$ V/cm, 585 V/cm, and 1.5 kV/cm for different magnetic fields and laser polarizations. These decay rates are indicative of the measured S_γ values. The calculations show that, for $|\Delta M_J| = 1$ transitions in magnetic fields below 1 kG, the quenching efficiency is always higher in the presence of an applied electric field.

Figure 12(a) shows measurements of electric-field-induced annihilation performed in two different magnetic fields. An interesting feature of these data is that when the magnetic field is increased to 150 G, the magnitude of the signal is not only scaled, but shifted towards positive values, eliminating any negative signal in the high-electric-field regions. It can also be seen from Fig. 12(b) that a similar effect is seen if the laser power is increased. This supports the suggestion that there may be optical pumping effects contributing to the signal.

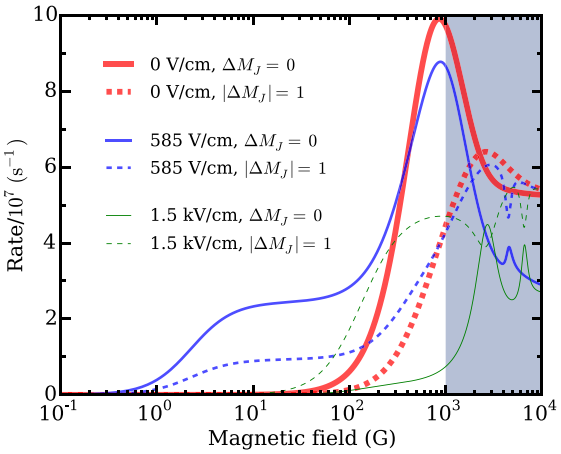

FIG. 11. Spectral-intensity-weighted average $n = 2$ fluorescence rates to the short-lived $1\,^1S_0$ level as a function of magnetic field when the excitation laser radiation is linearly polarized parallel (continuous lines) and perpendicular (dashed lines) to the magnetic field and $F = 0$ V/cm (red thick line), 585 V/cm (blue medium-thickness line), and 1.5 kV/cm (green thin line). In the shaded region spanning from 1 to 10 kG, the accuracy of the calculation is limited by Zeeman energy shifts in the ground state.

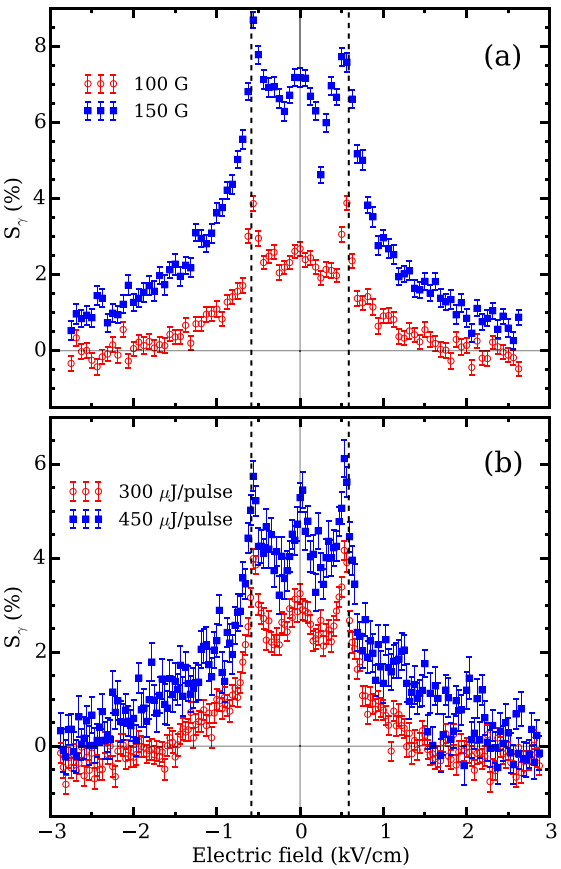

FIG. 12. The electric-field dependence of S_γ for photoexcitation via $\Delta M_J = 0$ transitions for (a) $B = 100$ G and $B = 150$ G and the laser pulse energy 800 μJ and (b) the laser pulse energy of 300 and 450 μJ when $B = 130$ G. In each case the cross-sectional area of the laser beam was approximately 0.5 cm^2.

V. CONCLUSIONS

The use of electric and magnetic fields to control atomic and molecular photoexcitation and decay pathways is well established and has many useful applications (e.g., [69–71]). We have shown that similar techniques may also be used to control the annihilation dynamics in Ps atoms. There are several areas where this is important: (1) in the optimization of multiphoton excitation of highly excited states, (2) to increase quenching rates for Ps detection, and (3) for the production of long-lived $2\,^3S_1$ levels via single-photon excitation.

From the results presented here it is clear that in experiments designed to prepare Rydberg-Stark states of Ps via a two-color two-step optical excitation in combined electric and magnetic fields, the evolution of the intermediate states should be taken into account [72]. Moreover, insofar as there may be loss mechanisms in the intermediate state (e.g., [73]), the increased Ps lifetimes of some mixed states could be utilized to enhance Rydberg Ps production.

If high Rydberg states [64] can be produced more efficiently using these approaches, then many other experimental areas may benefit, for example, electric-field control of the translational motion of Ps [72] or Ps scattering measurements, which are currently conducted using only ground-state atoms (e.g., [74,75]). Controlled and slowed Ps beams may also find application in the production of antihydrogen atoms [76–79], in Ps Bose-Einstein condensates [80–83], Ps gravity measurements [84,85], and in Ps spectroscopy and QED tests [86–89].

In a weak magnetic field one could rapidly switch an electric field to induce quenching. By switching the field from $F = 585$ V/cm to $F = 3$ kV/cm the quenching signal can be essentially turned on or off. Figure 13(a) shows spectra encompassing the $1\,^3S_1 \rightarrow 2\,^3P_J$ transitions that were measured in three different electric fields ($F = 0$, 585, and 3000 V/cm) with the UV laser radiation polarized linearly parallel to the z axis. In the highest of these fields we expect no quenching. Excitation of Ps atoms to $2\,^3P_J$ levels in fields that do not facilitate any quenching does not typically lead to any observable signal; $2\,^3P_J$ atoms generally do not annihilate (see Table I), but as they will decay back to the $1\,^3S_1$ level in 3.19 ns the net effect of excitation is a very small ($\sim$1%) increase in the total Ps lifetime. Under these conditions photoionization of the $2\,^3P_J$ atoms can be used to generate a γ-ray signal [as shown in Fig. 13(a), where controlled Stark mixing is directly compared to photoionization]. The cross section for this process is approximately 10^6 times lower than that of the $1\,^3S_1 \rightarrow 2\,^3P_J$ excitation [9], and for typical experimental conditions pulse energies of $\sim$10 mJ per pulse are required [90]. These high energies may not always be acceptable, for example in a cryogenic system, or if delicate Ps formation targets are used (e.g., [91]).

Photoionization can always be made more efficient than magnetic quenching (with or without Stark mixing) since one can saturate the process. However, from a practical point of view, it can be very convenient to optimize an excitation process via magnetic quenching, independently of any subsequent ionization process.

Efficient utilization of a photoionization signal requires that the liberated positron rapidly annihilates, or is otherwise detected. For some experiments long-lived Ps atoms might be transported to a region in which this is not possible, for example, if the electric field is zero, or if the positron is physically distant from any solid object or detector when it annihilates.

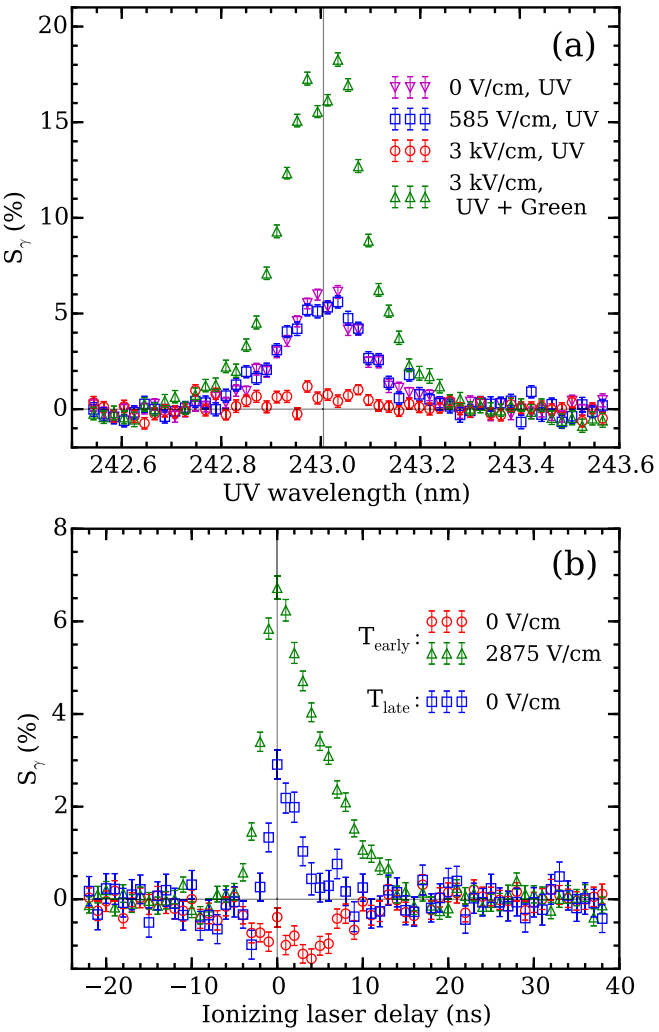

FIG. 13. (a) Spectra encompassing the $1\,^3S_1 \rightarrow 2\,^3P_J$ transitions in a range of electric fields. The data were recorded using laser radiation polarized parallel to the electric field ($\Delta M_J = 0$). For one scan (UV + green) a 532-nm photoionization laser was also present to directly compare magnetic quenching and ionization signals. The noticeable Lamb dip [59] in both the ionization and the quenching line shapes is attributed to UV radiation reflected from uncoated vacuum windows. (b) The dependence of S_γ on the delay between photoexcitation and photoionization. For each measurement the photoionization laser was tuned to the ionizing threshold (729 nm). The data analysis was performed using two sets of time windows, $T_{\rm early}$ and $T_{\rm late}$ (see text for details).

Figure 13(b) shows Ps photoionization data recorded in low ($F \simeq 0$ V/cm) and high ($F = 2875$ V/cm) electric fields. The slightly negative values for the zero-field case occur because the positrons are detected much later than f is sensitive to, when defined by the usual early time windows ($A_{\rm early} = -4$ ns, $B_{\rm early} = 35$ ns, $C_{\rm early} = 600$ ns). When time windows appropriate for delayed events are used ($A_{\rm late} =$

-4 ns, $B_{\text{late}} = 120$ ns, $C_{\text{late}} = 600$ ns) the signal is restored (see Sec. II B).

Relatively slow positrons are produced in this process, corresponding to the initial Ps kinetic energy of ∼50 meV (equivalent to speeds of approximately 10^7 cm/s), which is divided equally between the electron and the positron. For near-threshold ionization (using 729-nm radiation) the excess energy given to the electron-positron pair from the photon is negligible, whereas for 532-nm radiation this will amount to 300 meV per particle, along the direction of polarization of the laser radiation. Similar techniques are, in fact, used for the production of cold electron beams [92]. Since the UV laser bandwidth (85 GHz) corresponds to less than 1 meV, similar methods could be applied to the production of pulsed cold positron beams, although such velocity selection would likely be inefficient compared to existing trap-based methods [93]. Magnetic quenching would not act as a loss mechanism for any such scheme provided an ionization laser of sufficient power is employed.

Photoexcitation in the presence of electric fields $F \gtrsim 1$ kV/cm permits single-photon access to the outer Stark state that can be removed adiabatically from the field to produce atoms in $2\,^3S_1$ levels. Previously, $2\,^3S_1$ atoms have been produced by positron bombardment of untreated metal surfaces [94–97], or by two-photon ($1\,^3S_1 \rightarrow 2\,^3S_1$) excitation [6,98]. The former method is very inefficient (typically less than 0.1%), while the latter requires significant laser power. It would therefore be considerably more convenient to use a single-photon excitation scheme and then an appropriate field configuration to extract pure $2\,^3S_1$ atoms. From the data in Fig. 8(a) we estimate that ∼10% of atoms excited with the UV laser radiation polarized parallel to an electric field of ∼3 kV/cm are in the Stark eigenstate that adiabatically evolves to the $2\,^3S_1$ level in zero field. The availability of such atoms will facilitate microwave spectroscopy of the Ps $n = 2$ fine structure. Several such measurements have been conducted previously [99–101], all of them using the small fraction of collisionally produced $2\,^3S_1$ levels; the ability to optically produce $n = 2$ states with high efficiency will make it possible to revisit these measurements with greatly improved statistical limits. Combining velocity selection following single-photon excitation with trajectory mapping Doppler correction methods [102] could also provide enhanced precision.

Photoexcitation of Ps to $n = 2$ levels and manipulation of Stark and Zeeman mixing to either enhance magnetic quenching or increase the lifetime is, in both cases, incompatible with Ps laser cooling [103]. Magnetic quenching represents a severe loss mechanism, whereas increasing the fluorescence lifetime reduces the cooling rate. Ps laser cooling could, in principle, be accomplished in very low ($\lesssim$20 G) or very high ($\gtrsim$20 kG) magnetic fields since in these cases magnetic quenching is suppressed [14,15]. However, these fields are not particularly compatible with trap-based positron beams [32]. It is more common to use magnetic fields of ∼400–1000 G for beam transport and confinement, in which magnetic quenching effects are all but unavoidable if the electric fields are not properly chosen. However, as is evident from Fig. 5, exciting Ps atoms to sublevels with either $M_J = +2$ or $M_J = -2$ would not result in any singlet-triplet mixing, regardless of the magnetic field. Therefore, using these transitions, laser cooling would be possible for approximately 1/3 of the initial ensemble using circularly polarized light.

ACKNOWLEDGMENTS

The authors are grateful to T. E. Wall for prior work involving the laser setup and to L. Liszkay for providing silica samples. This work was supported by UCL through its Impact Studentship Programme and was funded in part by the Leverhulme trust (Grant No. RPG-2013-055), the ERC (Grant No. CIG 630119), and the EPSRC (Grant No. EP/K028774/1).

[1] J. A. Wheeler, Polyelectrons, Ann. N.Y. Acad. Sci. **48**, 219 (1946).
[2] M. Deutsch, Evidence for the formation of positronium in gases, Phys. Rev. **82**, 455 (1951).
[3] S. Berko and H. N. Pendleton, Positronium, Annu. Rev. Nucl. Part. Sci. **30**, 543 (1980).
[4] A. Rich, Recent experimental advances in positronium research, Rev. Mod. Phys. **53**, 127 (1981).
[5] D. W. Gidley, H. G. Peng, and R. S. Vallery, Positron annihilation as a method to characterize porous materials, Annu. Rev. Mater. Res. **36**, 49 (2006).
[6] S. Chu and A. P. Mills, Jr., Excitation of the Positronium $1^3S_1 \rightarrow 2^3S_1$ Two-Photon Transition, Phys. Rev. Lett. **48**, 1333 (1982).
[7] A. Badertscher, P. Crivelli, W. Fetscher, U. Gendotti, S. N. Gninenko, V. Postoev, A. Rubbia, V. Samoylenko, and D. Sillou, Improved limit on invisible decays of positronium, Phys. Rev. D **75**, 032004 (2007).
[8] R. A. Ferrell, The positronium fine structure, Phys. Rev. **84**, 858 (1951).
[9] H. A. Bethe and E. E. Salpeter, *Quantum Mechanics of One- and Two-Electron Atoms* (Springer, Berlin, 1957).
[10] M. Deutsch and S. C. Brown, Zeeman effect and hyperfine splitting of positronium, Phys. Rev. **85**, 1047 (1952).
[11] S. B. Crampton, D. Kleppner, and N. F. Ramsey, Hyperfine Separation of Ground-State Atomic Hydrogen, Phys. Rev. Lett. **11**, 338 (1963).
[12] *Positron Beams and Their Applications*, 1st ed., edited by P. G. Coleman (World Scientific, Singapore, 2000).
[13] T. Yamazaki, A. Miyazaki, T. Suehara, T. Namba, S. Asai, T. Kobayashi, H. Saito, I. Ogawa, T. Idehara, and S. Sabchevski, Direct Observation of the Hyperfine Transition of Ground-State Positronium, Phys. Rev. Lett. **108**, 253401 (2012).
[14] K. P. Ziock, C. D. Dermer, R. H. Howell, F. Magnotta, and K. M. Jones, Optical saturation of the $1^3S - 2^3P$ transition in positronium, J. Phys. B **23**, 329 (1990).
[15] D. B. Cassidy, T. H. Hisakado, H. W. K. Tom, and A. P. Mills, Jr., Laser Excitation of Positronium in the Paschen-Back Regime, Phys. Rev. Lett. **106**, 173401 (2011).

[16] P. A. M. Dirac, *The Principles of Quantum Mechanics* (Clarendon Press, Oxford, 1930).
[17] A. I. Alekseev, Two-photon annihilation of positronium in the P-state, Sov. Phys. JETP **7**, 826 (1958).
[18] J. Shapiro and G. Breit, Metastability of 2*s* states of hydrogenic atoms, Phys. Rev. **113**, 179 (1959).
[19] A. I. Alekseev, Three-photon annihilation of positronium in the P-state, Sov. Phys. JETP **9**, 1312 (1959).
[20] P. A. M. Dirac, On the annihilation of electrons and protons, Math. Proc. Cambridge Philos. Soc. **26**, 361 (1930).
[21] A. Ore and J. L. Powell, Three-photon annihilation of an electron-positron pair, Phys. Rev. **75**, 1696 (1949).
[22] P. Wallyn, W. A. Mahoney, P. Durouchoux, and C. Chapuis, The positronium radiative combination spectrum: Calculation in the limit of thermal positrons and low densities, Astrophys. J. **465**, 473 (1996).
[23] V. A. Pazdzerskii, Positronium annihilation in a strong electromagnetic field, Sov. Phys. J. **20**, 963 (1977).
[24] F. H. M. Faisal and P. S. Ray, Excitation and delayed annihilation of Ps in a laser field, J. Phys. B **14**, L715 (1981).
[25] M. H. Mittleman, Change of the annihilation rate of Ps in a resonant laser, Phys. Rev. A **33**, 2840 (1986).
[26] F. Ehlotzky, Positronium decay in intense high frequency laser fields, Phys. Lett. A **126**, 524 (1988).
[27] A. Karlson and M. H. Mittleman, Stabilization of positronium by laser fields, J. Phys. B **29**, 4609 (1996).
[28] L. B. Madsen, L. A. A. Nikolopoulos, and P. Lambropoulos, Efficient excitation of Ps by 50-100 fs laser pulses, J. Phys. B **32**, L425 (1999).
[29] F. M. S. Lima, M. A. Amato, O. A. C. Nunes, A. L. A. Fonseca, and E. F. da Silva, Jr., Increase of the positronium lifetime under high-frequency, intense laser fields, J. Phys. B **42**, 055601 (2009).
[30] N. Cui, M. Macovei, K. Z. Hatsagortsyan, and C. H. Keitel, Manipulating the Annihilation Dynamics of Positronium via Collective Radiation, Phys. Rev. Lett. **108**, 243401 (2012).
[31] A. M. Alonso, B. S. Cooper, A. Deller, S. D. Hogan, and D. B. Cassidy, Controlling Positronium Annihilation with Electric Fields, Phys. Rev. Lett. **115**, 183401 (2015).
[32] J. R. Danielson, D. H. E. Dubin, R. G. Greaves, and C. M. Surko, Plasma and trap-based techniques for science with positrons, Rev. Mod. Phys. **87**, 247 (2015).
[33] B. S. Cooper, A. M. Alonso, A. Deller, T. E. Wall, and D. B. Cassidy, A trap-based pulsed positron beam optimised for positronium laser spectroscopy, Rev. Sci. Instrum. **86**, 103101 (2015).
[34] D. B. Cassidy, S. H. M. Deng, R. G. Greaves, and A. P. Mills, Jr., Accumulator for the production of intense positron pulses, Rev. Sci. Instrum. **77**, 073106 (2006).
[35] D. B. Cassidy, P. Crivelli, T. H. Hisakado, L. Liszkay, V. E. Meligne, P. Perez, H. W. K. Tom, and A. P. Mills, Jr., Positronium cooling in porous silica measured via Doppler spectroscopy, Phys. Rev. A **81**, 012715 (2010).
[36] A. P. Mills, Jr., Time bunching of slow positrons for annihilation lifetime and pulsed laser photon absorption experiments, Appl. Phys. **22**, 273 (1980).
[37] L. Liszkay, C. Corbel, P. Perez, P. Desgardin, M. F. Barthe, T. Ohdaira, R. Suzuki, P. Crivelli, U. Gendotti, A. Rubbia, M. Etienne, and A. Walcarius, Positronium reemission yield from mesostructured silica films, Appl. Phys. Lett. **92**, 063114 (2008).
[38] L. Liszkay, M. F. Barthe, C. Corbel, P. Crivelli, P. Desgardin, M. Etienne, T. Ohdaira, P. Perez, R. Suzuki, V. Valtchev, and A. Walcarius, Orthopositronium annihilation and emission in mesostructured thin silica and silicalite-1 films, Appl. Surf. Sci. **255**, 187 (2008).
[39] L. Liszkay, F. Guillemot, C. Corbel, J.-P. Boilot, T. Gacoin, E. Barthel, P. Pérez, M.-F. Barthe, P. Desgardin, P. Crivelli, U. Gendotti, and A. Rubbia, Positron annihilation in latex-templated macroporous silica films: Pore size and orthopositronium escape, New J. Phys. **14**, 065009 (2012).
[40] P. Crivelli, U. Gendotti, A. Rubbia, L. Liszkay, P. Perez, and C. Corbel, Measurement of the orthopositronium confinement energy in mesoporous thin films, Phys. Rev. A **81**, 052703 (2010).
[41] A. Deller, B. S. Cooper, T. E. Wall, and D. B. Cassidy, Positronium emission from mesoporous silica studied by laser-enhanced time-of-flight spectroscopy, New J. Phys. **17**, 043059 (2015).
[42] H. Kanazawa, Y. H. Ohtsuki, and S. Yanagawa, Positronium formation in metals, Phys. Rev. **138**, A1155 (1965).
[43] P. J. Schultz and K. G. Lynn, Interaction of positron beams with surfaces, thin films, and interfaces, Rev. Mod. Phys. **60**, 701 (1988).
[44] F. Tuomisto and I. Makkonen, Defect identification in semiconductors with positron annihilation: Experiment and theory, Rev. Mod. Phys. **85**, 1583 (2013).
[45] L. Wolfenstein and D. G. Ravenhall, Some consequences of invariance under charge conjugation, Phys. Rev. **88**, 279 (1952).
[46] C. N. Yang, Selection rules for the dematerialization of a particle into two photons, Phys. Rev. **77**, 242 (1950).
[47] L. Michel, Selection rules imposed by charge conjugation, Il Nuovo Cimento (1943–1954) **10**, 319 (1953).
[48] S. Shimizu, T. Mukoyama, and Y. Nakayama, Radiationless annihilation of positrons in lead, Phys. Rev. **173**, 405 (1968).
[49] A. W. Hunt, D. B. Cassidy, F. A. Selim, R. Haakenaasen, T. E. Cowan, R. H. Howell, K. G. Lynn, and J. A. Golovchenko, Spatial sampling of crystal electrons by in-flight annihilation of fast positrons, Nature (London) **402**, 157 (1999).
[50] M. Deutsch, Three-quantum decay of positronium, Phys. Rev. **83**, 866 (1951).
[51] A. P. Mills, Jr., and P. M. Platzman, New experiments with bright positron and positronium beams, in *New Directions in Antimatter Chemistry and Physics*, edited by G. M. Surko and F. A. Gianturco (Kluwer, Dordrecht, 2001), pp. 115–126.
[52] M. Charlton and J. W. Humberston, *Positron Physics*, 1st ed., Cambridge Monographs on Atomic, Molecular and Chemical Physics Vol. II (Cambridge University Press, Cambridge, UK, 2001).
[53] R. Krause-Rehberg and H. S. Leipner, *Positron Annihilation in Semiconductors: Defect Studies*, Springer Series in Solid-State Sciences (Springer, Berlin Heidelberg, 2010).
[54] G. R. Gilmore, Electronics for gamma-ray spectrometry, in *Practical Gamma-Ray Spectrometry* (Wiley & Sons, New York, 2008), pp. 61–99.
[55] K. P. Ziock, R. H. Howell, F. Magnotta, R. A. Failor, and K. M. Jones, First Observation of Resonant Excitation of High-*n* States in Positronium, Phys. Rev. Lett. **64**, 2366 (1990).

[56] D. B. Cassidy, S. H. M. Deng, H. K. M. Tanaka, and A. P. Mills, Jr., Single shot positron annihilation lifetime spectroscopy, Appl. Phys. Lett. **88**, 194105 (2006).

[57] D. B. Cassidy and A. P. Mills, Jr., A fast detector for single-shot positron annihilation lifetime spectroscopy, Nucl. Instrum. Methods Phys. Res., Sect. A **580**, 1338 (2007).

[58] D. B. Cassidy, T. H. Hisakado, H. W. K. Tom, and A. P. Mills, Jr., Positronium formation via excitonlike states on Si and Ge surfaces, Phys. Rev. B **84**, 195312 (2011).

[59] W. Demtröder, *Laser Spectroscopy*, 3rd ed. (Springer, New York, 2003).

[60] D. B. Cassidy, T. H. Hisakado, H. W. K. Tom, and A. P. Mills, Jr., Positronium Hyperfine Interval Measured via Saturated Absorption Spectroscopy, Phys. Rev. Lett. **109**, 073401 (2012).

[61] S. M. Curry, Combined Zeeman and motional Stark effects in the first excited state of positronium, Phys. Rev. A **7**, 447 (1973).

[62] C. D. Dermer and J. C. Weisheit, Perturbative analysis of simultaneous Stark and Zeeman effects on $n = 1 \leftrightarrows n = 2$ radiative transitions in positronium, Phys. Rev. A **40**, 5526 (1989).

[63] A. Ishida, T. Namba, S. Asai, T. Kobayashi, H. Saito, M. Yoshida, K. Tanaka, and A. Yamamoto, New precision measurement of hyperfine splitting of positronium, Phys. Lett. B **734**, 338 (2014).

[64] T. F. Gallagher, *Rydberg Atoms* (Cambridge University Press, Cambridge, 1994).

[65] N. Overton and P. G. Coleman, Measurement of the Energy Spectrum of Secondary Electrons Ejected from Solids by Positron Impact, Phys. Rev. Lett. **79**, 305 (1997).

[66] C. P. Hauri, R. Ganter, F. Le Pimpec, A. Trisorio, C. Ruchert, and H. H. Braun, Intrinsic Emittance Reduction of an Electron Beam from Metal Photocathodes, Phys. Rev. Lett. **104**, 234802 (2010).

[67] J. Wheatley and D. Halliday, The quenching of *ortho*-positronium decay by a magnetic field, Phys. Rev. **88**, 424 (1952).

[68] A. Deller, D. Edwards, T. Mortensen, C. A. Isaac, D. P. van der Werf, H. H. Telle, and M. Charlton, Exciting positronium with a solid-state UV laser: the Doppler-broadened Lyman-α transition, J. Phys. B **48**, 175001 (2015).

[69] B. R. Johnson, J. O. Hirschfelder, and K. Yang, Interaction of atoms, molecules, and ions with constant electric and magnetic fields, Rev. Mod. Phys. **55**, 109 (1983).

[70] A. Derevianko and H. Katori, *Colloquium*: Physics of optical lattice clocks, Rev. Mod. Phys. **83**, 331 (2011).

[71] C. Zimmermann, R. Kallenbach, and T. W. Hänsch, High-Resolution Spectroscopy of the Hydrogen $1S \rightarrow 2S$ Transition in an Atomic Beam, Phys. Rev. Lett. **65**, 571 (1990).

[72] T. E. Wall, A. M. Alonso, B. S. Cooper, A. Deller, S. D. Hogan, and D. B. Cassidy, Selective Production of Rydberg-Stark States of Positronium, Phys. Rev. Lett. **114**, 173001 (2015).

[73] F. Castelli, I. Boscolo, S. Cialdi, M. G. Giammarchi, and D. Comparat, Efficient positronium laser excitation for antihydrogen production in a magnetic field, Phys. Rev. A **78**, 052512 (2008).

[74] S. J. Brawley, S. Armitage, J. Beale, D. E. Leslie, A. I. Williams, and G. Laricchia, Electron-like scattering of positronium, Science **330**, 789 (2010).

[75] M. Shipman, S. Armitage, J. Beale, S. J. Brawley, S. E. Fayer, A. J. Garner, D. E. Leslie, P. Van Reeth, and G. Laricchia, Absolute Differential Positronium-Formation Cross Sections, Phys. Rev. Lett. **115**, 033401 (2015).

[76] A. S. Kadyrov, C. M. Rawlins, A. T. Stelbovics, I. Bray, and M. Charlton, Antihydrogen Formation via Antiproton Scattering with Excited Positronium, Phys. Rev. Lett. **114**, 183201 (2015).

[77] P. Perez and Y. Sacquin, The GBAR experiment: Gravitational behavior of antihydrogen at rest, Classical Quantum Gravity **29**, 184008 (2012).

[78] A. Kellerbauer *et al.*, Proposed antimatter gravity measurement with an antihydrogen beam, Nucl. Instrum. Methods Phys. Res., Sect. B **266**, 351 (2008).

[79] C. H. Storry, A. Speck, D. Le Sage, N. Guise, G. Gabrielse, D. Grzonka, W. Oelert, G. Schepers, T. Sefzick, H. Pittner, M. Herrmann, J. Walz, T. W. Hänsch, D. Comeau, and E. A. Hessels (ATRAP Collaboration), First Laser-Controlled Antihydrogen Production, Phys. Rev. Lett. **93**, 263401 (2004).

[80] P. M. Platzman and A. P. Mills, Jr., Possibilities for Bose condensation of positronium, Phys. Rev. B **49**, 454 (1994).

[81] D. B. Cassidy, V. E. Meligne, and A. P. Mills, Jr., Production of a Fully Spin-Polarized Ensemble of Positronium Atoms, Phys. Rev. Lett. **104**, 173401 (2010).

[82] Y.-H. Wang, B. M. Anderson, and C. W. Clark, Spinor Bose-Einstein condensates of positronium, Phys. Rev. A **89**, 043624 (2014).

[83] H. K. Avetissian, A. K. Avetissian, and G. F. Mkrtchian, Self-Amplified Gamma-Ray Laser on Positronium Atoms from a Bose-Einstein Condensate, Phys. Rev. Lett. **113**, 023904 (2014).

[84] A. P. Mills, Jr., and M. Leventhal, Can we measure the gravitational free fall of cold Rydberg state positronium?, Nucl. Instrum. Methods Phys. Res., Sect. B **192**, 102 (2002).

[85] D. B. Cassidy and S. D. Hogan, Atom control and gravity measurements using Rydberg positronium, Int. J. Mod. Phys.: Conf. Ser. **30**, 1460259 (2014).

[86] S. G Karshenboim, Precision study of positronium: Testing bound state qed theory, Int. J. Mod. Phys. A **19**, 3879 (2004).

[87] M. S. Fee, A. P. Mills, Jr., S. Chu, E. D. Shaw, K. Danzmann, R. J. Chichester, and D. M. Zuckerman, Measurement of the Positronium 1^3S_1-2^3S_1 Interval by Continuous-Wave Two-Photon Excitation, Phys. Rev. Lett. **70**, 1397 (1993).

[88] S. G. Karshenboim, Precision physics of simple atoms: QED tests, nuclear structure and fundamental constants, Phys. Rep. **422**, 1 (2005).

[89] R. Pohl, R. Gilman, G. A. Miller, and K. Pachucki, Muonic hydrogen and the proton radius puzzle, Annu. Rev. Nucl. Part. Sci. **63**, 175 (2013).

[90] M. S. Fee, A. P. Mills, Jr., E. D. Shaw, R. J. Chichester, D. M. Zuckerman, S. Chu, and K. Danzmann, Sensitive detection of Doppler-free two-photon-excited 2 *S* positronium by spatially separated photoionization, Phys. Rev. A **44**, R5 (1991).

[91] S. L. Andersen, D. B. Cassidy, J. Chevallier, B. S Cooper, A. Deller, T. E Wall, and U. I. Uggerhøj, Positronium emission and cooling in reflection and transmission from thin meso-structured silica films, J. Phys. B **48**, 204003 (2015).

[92] A. C. Gallagher and G. York, A photoionization source of monoenergetic electrons, Rev. Sci. Instrum. **45**, 662 (1974).

[93] S. J. Gilbert, C. Kurz, R. G. Greaves, and C. M. Surko, Creation of a monoenergetic pulsed positron beam, Appl. Phys. Lett. **70**, 1944 (1997).

[94] K. F. Canter, A. P. Mills, Jr., and S. Berko, Observations of Positronium Lyman-α Radiation, Phys. Rev. Lett. **34**, 177 (1975).

[95] T. D. Steiger and R. S. Conti, Formation of $n = 2$ positronium from untreated metal surfaces, Phys. Rev. A **45**, 2744 (1992).

[96] D. C. Schoepf, S. Berko, K. F. Canter, and P. Sferlazzo, Observation of Ps($n = 2$) from well-characterized metal surfaces in ultrahigh vacuum, Phys. Rev. A **45**, 1407 (1992).

[97] D. J. Day, M. Charlton, and G. Laricchia, On the formation of excited state positronium in vacuum by positron impact on untreated surfaces, J. Phys. B **34**, 3617 (2001).

[98] D. A. Cooke, P. Crivelli, J. Alnis, A. Antognini, B. Brown, S. Friedreich, A. Gabard, T.W. Haensch, K. Kirch, A. Rubbia, and V. Vrankovic, Observation of positronium annihilation in the $2S$ state: Towards a new measurement of the $1S$-$2S$ transition frequency, Hyperfine Interact. **233**, 67 (2015).

[99] A. P. Mills, Jr., S. Berko, and K. F. Canter, Fine-Structure Measurement in the First Excited State of Positronium, Phys. Rev. Lett. **34**, 1541 (1975).

[100] S. Hatamian, R. S. Conti, and A. Rich, Measurements of the 2^3S_1-2^3P_J ($J = 0,1,2$) Fine-Structure Splittings in Positronium, Phys. Rev. Lett. **58**, 1833 (1987).

[101] D. Hagena, R. Ley, D. Weil, G. Werth, W. Arnold, and H. Schneider, Precise Measurement of $n = 2$ Positronium Fine-Structure Intervals, Phys. Rev. Lett. **71**, 2887 (1993).

[102] A. C. L. Jones, T. H. Hisakado, H. J. Goldman, H. W. K. Tom, A. P. Mills, Jr., and D. B. Cassidy, Doppler-corrected Balmer spectroscopy of Rydberg positronium, Phys. Rev. A **90**, 012503 (2014).

[103] E. P. Liang and C. D. Dermer, Laser cooling of positronium, Opt. Commun. **65**, 419 (1988).